Geophysical Journal International Advance Access published October 23, 2016

Effect of soil and bedrock anelasticity on the S-wave amplification function

José M. Carcione[1], Stefano Picotti[1], Roberto Francese[2], Massimo Giorgi[1], Franco Pettenati[1]
[1]*Istituto Nazionale di Oceanografia e di Geofisica Sperimentale - OGS - Borgo Grotta Gigante 42/c, 34010, Sgonico (Trieste), ITALY.*
[2]*University of Parma, ITALY.*
Correspondence: Stefano Picotti <jcarcione@inogs.it>

Received 2016 April 20

SUMMARY
We analyze how intrinsic attenuation and bedrock elasticity affect the amplitude and frequency of the resonance peaks of the S-wave amplification function. The Zener model (with a single relaxation peak) and the constant-Q model are used to describe attenuation. We consider two different cases, namely, the soil is softer than the bedrock (the usual situation, that is, a sediment overlying a stiff formation) and the upper layer is stiffer than the lower half space (e.g., basalt over sediment). The presence of Zener loss in the upper layer causes a shift of the fundamental peak towards the low frequencies, while no shift is observed due to the non-rigid (viscoelastic) character of the half space. In the constant-Q case, the shift to the low frequencies is not significant implying that it is difficult to estimate the attenuation parameters on the basis of the location of the resonance peaks. However, attenuation affects the amplitude of the higher modes, while these modes have the same amplitude of the fundamental mode no matter the degree of elasticity of the half space. Attenuation of the layer and non-rigidity of the half space affect the peaks, with the latter having a stronger effect. Examples are given, where we consider two real cases representing a glacier and an ice stream in Northern Italy and the Antarctic continent, respectively.

Key words: Amplification function – S-waves – anelasticity – glaciers.

1 INTRODUCTION

We analyse the effects of soil and bedrock anelasticity on the S-wave amplification function, i.e., how anelasticity affects the amplitude and frequency of the resonance peaks. The amplification function is an essential concept in the horizontal to vertical spectral ratio (HVSR) method, originally introduced by Nogoshi and Igarashi (1971). The method is based on the frequency spectrum obtained by dividing the horizontal component by the vertical component (H/V ratio), either displacement, particle velocity or acceleration, since the results are equivalent. The source can be ambient noise, earthquakes or active sources of different nature. It has been shown that for shear and Rayleigh waves propagating in a layer over a half space, the methods yields the fundamental resonance frequency and the related amplitude (Lermo and Chávez García, 1993; Lunedei and Malischewsky, 2015).The investigations suggest that the H/V ratio provides a reliable approximation of the site S-wave transfer function. If the ratio is controlled by the fundamental Rayleigh waves, there is only an indirect correlation between the H/V peak amplitude and the site amplification (Bonnefoy-Claudet et al., 2006). A more detailed study of the influence of surface and body waves by varying several parameters is given in Albarello and Lunedei (2011). A case study is proposed in D'Amico et al. (2008), where a first-order reconstruction of the seismic bedrock topography shows a good consistency with available geological/log data.

The first significant and detailed theoretical tests of the method have been performed by Konno and Ohmachi (1998) who show that the H/V ratio is related to the fundamental-mode Rayleigh wave regarding its resonant frequency and to the S-wave amplification function. More detailed viscoelastic numerical tests regard the SESAME project, whose results can mainly be found in Bonnefoy-Claudet et al. (2006). They have considered 1D plane-layered models and sources randomly distributed near the surface, i.e., impulsive and continuous (machines). The H/V ratio predicts the resonance frequency of the 1D transfer function corresponding to a vertically incident S-wave. Van der Baan (2009) explains the resonances obtained from the H/V ratio as due to SH and Love waves but in general these depend on several factors, such as the type of source, medium properties, interface geometry, etc.

The equation used to obtain the amplification function is usually based on a lossless soil overlying a rigid bedrock. Here, we study the effects of soil and bedrock anelasticity on the amplification function of shear waves, i.e., the presence of attenuation in the layer and half space and the fact the latter is deformable, i.e, viscoelastic and not rigid. Kramer (1996) provides the relevant equations of the amplification function, which is the ratio of the free surface motion amplitude to the bedrock motion amplitude, where viscoelasticity is described by a Kelvin-Voigt solid. Here, we use the Zener and constant-Q models to describe attenuation (e.g., Carcione, 2014), a more realistic description for rocks than the Kelvin-Voigt solid, which gives an infinite velocity at high frequencies. More complex models could be used, such as that of Albarello and Lunedei (2015), which considers the whole wavefield or the diffusive wavefield theory (Kawase et al., 2011; Sánchez-Sesma et al., 2011; García Jerez et al., 2013; Kawase et al., 2015). However, Kramer's equation satisfactory explains the physics involved in the examples presented here, namely, two real cases representing a glacier and an ice stream in Northern Italy and the Antarctic continent, respectively (Picotti et al., 2016). Although the theory is applied to glaciers, it can be used for other environments, where the geology can be represented by a flat layer over a half-space, both isotropic and anelastic.

2 SITE AMPLIFICATION FUNCTION

The body S-wave transfer function for a lossy sediment layer (soil) of thickness h over a viscoelastic bedrock describes the ratio of displacement amplitudes between the top and bottom of the layer due to horizontal harmonic motions of the bedrock. Let us define the layer (i = 1) and half space (i = 2) complex (Zener) shear-wave velocities as v_i, where

$$v = c_R\sqrt{\frac{1+\mathrm{i}\omega\tau a}{1+\mathrm{i}\omega\tau/a}} = c_U\sqrt{\frac{\mathrm{i}\omega\tau+1/a}{\mathrm{i}\omega\tau+a}}, \quad a=\frac{c_U}{c_R}\geq 1, \tag{1}$$

where c_R and c_U are the low (relaxed)- and high (unrelaxed)-frequency limit velocities, ω is the angular frequency, $f = 1/(2\pi\tau)$ is the centre frequency of the relaxation peak and $\mathrm{i} = \sqrt{-1}$. The peak quality factor is given by $Q = 2(1-1/a)^{-1}$. Therefore, the properties f, c_U and Q define the media, where $a = Q^{-1} + \sqrt{1+Q^{-2}}$ (e.g., Carcione, 2014). When $c_R = c_U$ we have the lossless case, i.e., a = 1, $Q = \infty$ and $v = c_U$. We define the lossless case for $\omega \to \infty$, when $v \to c_U$. If ω = 0 we have $v = c_R = c_U/a$.

The transfer function is

$$F(\omega) = \left[\cos\left(\frac{\omega h}{v_1}\right) + \mathrm{i}\left(\frac{\rho_1 v_1}{\rho_2 v_2}\right)\sin\left(\frac{\omega h}{v_1}\right)\right]^{-1} \tag{2}$$

(Takahashi and Hirano 1941; Kramer, 1996, eq. 7.26), where ρ_i denotes the mass density. The site amplification function is merely $|F|$. A rigid bedrock is obtained for $\rho_2 v_2 \to \infty$. In this case and in the absence of loss, we have the following resonance frequencies when the cosine vanishes,

$$f_n = (2n+1)f_0,\ n=0,1,2,\ldots,\quad f_0=\frac{c_{U1}}{4h}. \tag{3}$$

Infinite amplitude values are obtained at these resonance frequencies. An analysis of the transfer function at the fundamental frequency is given in Appendix A.

3 RESULTS

We consider two main cases and study the location and amplitude of the fundamental mode (n = 0). The cases are:

Case 1: The layer (sediment) is softer than the half space (bedrock) (e.g., sediment over hard rock). 1.1: The impedance contrast is constant and we vary the loss properties. 1.2: The loss properties are constant and we vary the impedance contrast.

Case 2: The layer (hard rock) is stiffer than the half space (sediment) (e.g., basalt over sediment). 2.1: The impedance contrast is constant and we vary the loss properties. 2.2: The loss properties are constant and we vary the impedance contrast.

Let us consider a sediment with c_{U1} = 1 km/s, ρ_1 = 2 g/cm^3, Q_1 = 10 and h = 1 km. The impedance contrast is defined as

$$\alpha = \frac{\rho_1 c_{U1}}{\rho_2 c_{U2}}, \tag{4}$$

i.e., α = 0 yields maximum impedance contrast and α = 1 yields no contrast. Note that equation (2) depends on the lower medium through the impedance $I_2 = \rho_2 c_{U2}$. All the calculations consider $\tau = 1/(2\pi)$, i.e., the relaxation peak is centered at a frequency of 1 Hz. In the lossless-rigid case ($Q_1 = \infty$ and α = 0), we have f_n = 0.25 Hz, 0.75 Hz, 1.25 Hz, 1.75 Hz, ... Generally, the spectra are compared to that of the lossless-rigid case, which is the case mostly used to interpret H/V seismic responses.

3.1 Case 1. Soft layer over stiff half space

Case 1.1: Let us assume α = 0.3 and Q_2 = 50. The solid and dashed lines in Figure 1 correspond to the lossless-elastic and lossless-rigid cases, respectively (in this case, $Q_2 = \infty$). The peak in the second case is truncated since it reaches infinite values. The location of the peak is the same in both cases.

⟨⟨ Figure 1 ⟩⟩

The lossy case is given in Figure 2, where the higher resonances are damped. The comparison of Figures 1 and 2 shows that the presence of loss in the soil produces a shift of the peak towards the left side of the spectrum. If the Zener peak is located at frequencies lower than the fundamental-mode frequency, the shift is smaller, since the resonance peaks "see" the unrelaxed velocity c_U (the velocity related to the lossless case by definition), while there is a bigger shift if the Zener peak is located at higher frequencies compared to the fundamental one. In this case, the resonance peaks “see” the relaxed velocity c_R, which is smaller than c_U.

⟨⟨ Figure 2 ⟩⟩

The effects of bedrock elasticity and soil attenuation are similar. A stiffer bedrock means greater amplification as well as a less attenuating soil has the same effect. Figure 3 compares the lossy and elastic (non-rigid) cases (solid and dashed lines, respectively), where the amplification factor of the fundamental mode is the same. The effects can be discriminated on the basis of the location of the peak (although there is a small difference) and mainly on the behaviour of the higher modes.

⟨⟨ Figure 3 ⟩⟩

An elastic bedrock has a significant effect on the amplitude as can be seen in Figure 4, where the curve is compared to the rigid case with attenuation in the sediment. If Q_1 = 3 the fundamental mode moves to the left compared to Q_1 = 10 as expected and the higher resonances shows a larger shift and stronger attenuation (see Figure 5). However, the amplitude of the fundamental mode is not affected.

⟨⟨ Figure 4 ⟩⟩

⟨⟨ Figure 5 ⟩⟩

If there is no intrinsic loss, the amplification of the fundamental and higher modes is similar, as can be appreciated in Figure 3 (dashed line), but the elasticity of the bedrock is a more significant damper of the fundamental mode than intrinsic attenuation, which affects mainly the higher modes.

Case 1.2: Let us consider the lossless case ($Q_1 = Q_2 = \infty$) and the lossy case (Q_1 = 10, Q_2 = 50) and vary the impedance contrast α between 0 (rigid) and 0.8 (very deformable bedrock) in steps of 0.2. The results are shown in Figure 6. Clearly, the peak location is the same in the lossless case as the impedance contrast varies, while the presence of attenuation implies a shift of the peaks and attenuation of the higher modes.

⟨⟨ Figure 6 ⟩⟩

3.2 Case 2. Stiff layer over soft half space

Case 2.1: The layer is a stiff medium with a density ρ_1 = 2.5 g/cm^3 and Q_1 = 50, and the lower half-space has the properties of the soil, i.e., c_{U2} = 1 km/s and ρ_2 = 2 g/cm^3. We assume a constant impedance contrast α = 2, so that c_{U1} = 1.6 km/s. Figure 7 shows the amplification function for the lossless ($Q_2 = \infty$) and lossy cases (dotted and solid lines, respectively). There is damping in the latter case.

⟨⟨ Figure 7 ⟩⟩

Let us assume three values of Q_2, i.e., Q_2 = 10, 5 and 3. The amplification function shown in Figure 8a does not show significant variations as the Q factor of the half-space decreases. On the other hand, varying the Q factor of the layer and taking Q_2 = 10 the curves show remarkable differences (see Figure 8b).

⟨⟨ Figure 8 ⟩⟩

Case 2.2: The layer is a stiff medium with a density ρ_1 = 2.5 g/cm^3 and Q_1 = 50, and the lower half-space has c_{U2} = 1 km/s, ρ_2 = 2 g/cm^3 and Q_2 = 10. In this case, we assume the impedance contrast α = 2, 5 and 10, such that the velocity of the layer takes the values c_{U1} = 1.6, 4 and 8 km/s, respectively. Figure 9 shows the amplification function for each value of α. The modes shift to the higher frequencies and the spectrum stretches as the impedance contrast increases, i.e., the separation between modes increases.

⟨⟨ Figure 9 ⟩⟩

All these cases show a minimum of the transfer function at the fundamental frequency, as explained in Appendix A.

3.3 Effects of the attenuation model

The effect of the frequency dependence of the attenuation is analyzed by assuming a constant-Q model. This model has a simple expression of the complex velocity $v = c_U\sqrt{1 + \mathrm{i}/Q}$, such that the phase velocity and quality factor are frequency independent and equal to $1/\mathrm{Re}(1/v) > c_U$ and $\mathrm{Re}(v^2)/\mathrm{Im}(v^2) = Q$ over the whole frequency range. Since this velocity is greater than the lossless velocity c_U, it is expected a shift of the resonance peaks towards the high frequencies, i.e., the opposite effect compared to the Zener model. However, no significant shift is observed with respect to the ideal lossless-rigid case, as can be seen in Figure 10, corresponding to the lossy-elastic case represented in Figure 2 (we assume the same values for Q, i.e., Q_1 = 10 and Q_2 = 50). We can see that the modes have been attenuated compared to the Zener model.

⟨⟨ Figure 10 ⟩⟩

As stated above, the location of the Zener relaxation peak affects the location of the fundamental mode. Figure 11 displays the amplification function for the Zener relaxation peaks located at 0.05 Hz and 1 Hz, to the left and right of the fundamental mode in the lossless-rigid case. As can be seen, when the Zener relaxation peak is located at the left side, the shift is minimal, since the resonance modes "see" the lossless velocity c_U.

⟨⟨ Figure 11 ⟩⟩

It can be shown that in this case (rigid bedrock) there is no shift with respect to the ideal lossless-rigid case. Summarizing, the frequency dependence of the attenuation factor affects the amplitude and location of the modes, so that each case needs a specific calculation.

3.4 Real cases: Alpine glacier and Antarctic ice stream

We consider two real cases, with attenuation described by the constant-Q model (use of the Zener model yields similar results). Picotti et al. (2016) applied active seismics, radio echo sounding and geoelectric methods to verify the HVSR technique on Alpine glaciers and on a fast flowing ice stream of West Antarctica. In that work, the passive seismic measurements were carried out using different broadband seismometers, i.e., a Guralp, a Lennartz and a Trillium. The H/V spectra were obtained by performing a statistical analysis of the recorded wavefields in the frequency domain using the free software GEOPSY (http://www.geopsy.org – SESAME Project), whose details can be found in Picotti et al. (2016). The software computes the amplitude spectra of the three components in selected time windows, whose width depends on the target frequency band and on the record length. The window selection criterion is based on the quasi-stationarity of the signal amplitude. For the computation of the H/V ratio, the amplitude spectra of the horizontal components are combined using vector summation. Picotti et al. (2016) compared the results obtained from different geophysical methods, showing that the resonance frequency in the H/V spectra can be well correlated with the ice thickness at the site, in a wide range from tens of meters to over 800 m. However, a theoretical interpretation of these results is required to understand how the H/V spectra change in the presence of a deformable basement. Here we consider two of the experiments of Picotti et al. (2016), carried out on the Pian di Neve glacier (Italy) and on the Whillans Ice Stream (WIS - West Antarctica).

The Pian di Neve glacier occupies a high altitude 18 km^2 plateau in the Lombardy side of the Adamello massif. In October 2014, a 1-km active multichannel seismic survey has been carried out on this glacier (Picotti et al., 2016) to image the bedrock and the basal moraine and obtain the ice thickness profile. The imaging shows a smooth basement and the average thickness obtained from active seismic data is approximately h = 250 m. Picotti et al. (2016) also carried out several passive seismic experiments using different sensors in different periods, reporting a good stability of the measured fundamental resonant frequency in the H/V spectra. Under the hypothesis of an underlying rigid bedrock, they show a good correspondence between the thickness obtained from the resonance frequency and that obtained from the imaging. Here we want to verify, in this case, the reliability of the lossless-rigid assumption.
The average P-wave velocity of the bedrock (4500 m/s) obtained from the imaging is consistent with the in-situ types of rocks, which consist mainly of granitoid plutons compatible with the quartz-diorite (Blundy and Sparks, 1992). Typical values of the P- to S-wave velocity ratio R_v for such fractured crystalline basins is around 1.6 (Moos and Zoback, 1983), which yields an S-wave velocity for the bedrock of about c_{U2} = 2812 m/s. Moreover, the average density and quality factor of the bedrock can be assumed to be about 2700 kg/m^3 (Hughes, 1982) and Q_2 = 150 (Lay and Wallace, 1995), respectively. The average ice density is ρ_1 = 917 kg/m^3, while the average ice S-wave velocity obtained from the imaging is c_{U1} = 1860 m/s (Picotti et al., 2015; 2016). A reliable approximation of the ice S-wave quality factor can be computed using the following relationship

$$Q_1 = \frac{4}{3}\frac{Q_P}{R_v^2} \tag{5}$$

(Waters, 1978; Udias, 1999), where the ice P-wave quality factor Q_P ranges from 70 to 200 in temperate environments (Peters et al., 2012). Considering that the value of R_v for ice determined by Picotti et al. (2016) on the Pian di Neve glacier is about 2, the local average ice S-wave quality factor can be assumed $Q_1 \approx 50$. Figure 12 shows the experimental H/V response (a) and theoretical amplification function for the first three modes (b) using the lossy-elastic and lossless-rigid models. The colored curves in Figure 12a represent the H/V spectra obtained in each window selected for the statistical analysis. The black curve represents the H/V spectrum obtained as geometrical average of all the colored H/V curves. The two dashed lines represent the H/V standard deviation, while the grey areas represent the peak frequency standard deviation, and quantifies the experimental error associated to the average peak frequency value (located at the limit between the dark grey and light grey areas). On the other hand, the modeled higher modes shown in Figure 12b are damped with respect to the fundamental mode. The relevant result is that for both the two considered models the theory agrees, within the experimental errors, with the measured fundamental resonance frequency given by the H/V peak. Differences can be due to contributions of surface waves and the fact that the H/V response is not the amplification function in terms of amplitudes. However, the small discrepancy indicates that the fundamental peak is mainly due to S body waves. Therefore, in this case the lossless-rigid assumption used by Picotti et al. (2016) for the computation of the glacier thickness is valid. Moreover, the measured data show a second peak at $\approx$ 6 Hz, which corresponds to the first higher mode according to Figure 12b.

⟨⟨ Figure 12 ⟩⟩

The second real example is the WIS, a fast flowing ice stream feeding the Ross Ice Shelf from the interior of the West Antarctic Ice Sheet. Active seismic experiments (e.g., Blankenship et al., 1986; Picotti et al., 2015), as well as glaciological drilling and recordings (Engelhardt and Kamb, 1997), show the presence of highly deformable sediments and water beneath the WIS. These experiments also discovered the presence of Subglacial Lake Whillans (Horgan et al., 2012; Tulaczyk et al., 2014). Picotti et al. (2016) analyzed the H/V spectra obtained from the three-component seismic data recorded on the WIS by Picotti et al. (2015). The spectra show an average resonance peak at approximately 1.3 Hz. However, contrary to the previous case, the hypothesis of underlying rigid bedrock cannot be used to relate this frequency to the average ice thickness. Here we want to show that, in this case, the lossless-rigid assumption is actually inappropriate.

The thickness of WIS at the survey location is h = 780 m (Horgan et al., 2012), while the shallow firn layer is about 60 m thick (Picotti et al., 2015), implying that the average ice thickness below the firn is approximately 720 m. Moreover, the ice stream has c_{U1} = 1940 m/s, ρ_1 = 917 kg/m^3 and $R_v = 1.97$ (Picotti et al., 2015). Because in West Antarctica the ice Q_P ranges from 400 to 700 (Peters et al., 2012), it follows from equation (5) that the local average S-wave quality factor can be assumed $Q_1 \approx 200$. Blankenship et al. (1986) show that the S-wave velocity and density of the sediments below the WIS are approximately c_{U2} = 150 m/s and ρ_2 = 2016 kg/m^3, respectively, which are compatible with a highly dilated and deforming material. The quality factor of such soft sediments can be assumed $Q_2 \approx 10$ (Lay and Wallace, 1995). Figure 13 shows the experimental H/V response (a) and theoretical amplification function for the first three modes (b) using the lossy-elastic and lossless-rigid models. Again, the modeled higher modes are damped with respect to the fundamental mode, but attenuation does not affect the resonance frequencies (i.e., the peak positions) significantly.

Contrary to the previous case, the theory predicts the measured H/V peak only for the lossy-elastic model. In fact, Figure 13b shows that adopting the lossless-rigid approximation, the peak frequency is approximately 0.68 Hz, well outside the experimental error bounds. As explained in Appendix A and shown in subsection 3.2, this is due to the fact that when $\alpha \geq 1$ (stiff over soft medium) we have a minimum of the transfer function at the fundamental frequency f_0, and the first maximum is at $f_1 = 2f_0$. Thus, in this case assuming f_0 located at the H/V peak and using the lossless-rigid approximation will result in a wrong estimation of the glacier thickness.

⟨⟨ Figure 13 ⟩⟩

4 CONCLUSIONS

We study the effects of soil and bedrock anelasticity on the S-wave amplification function, i.e., how attenuation and bedrock deformability affect the amplitude and frequency of the resonance peaks. The Zener model is used to describe attenuation, with a single relaxation peak. We consider two different cases to study the location and amplitude of the fundamental mode, namely, the soil is softer than the bedrock (e.g., sediment over hard rock) and the layer is stiffer than the half space (e.g., basalt over sediment).

In the first case, the presence of loss in the soil causes a shift of the peak towards the low frequencies, where the amount of shift depends on the location of the Zener relaxation peak compared to the fundamental-mode resonant frequency. Damping is caused either by attenuation or by elasticity of the bedrock, with the last effect dominating. Damping of the higher modes is noticeable when there is strong attenuation, mainly that of the layer. However, the half space elasticity affects uniformly all the modes, i.e., their amplitudes are similar. In the second case (softer bedrock with a given impedance), the modes shift to the higher frequencies and the spectrum stretches as the impedance contrast increases, i.e., the separation between modes increases. Moreover, the transfer function shows a minimum at the fundamental frequency.

To analyze the effect of the frequency dependence of attenuation, we have considered a constant Q model. It is shown that the attenuation model affects the amplitude and location of the modes, so that each case needs an specific calculation. Finally, we consider two real cases in Northern Italy and the Antarctic continent, where the upper layer is ice, showing the prediction capabilities of the theory. In the latter case a very soft half space (sediment) below ice yields a minimum at the fundamental frequency and a resonance peak at higher frequencies compared to a rigid half space. Therefore, attenuation and bedrock elasticity must be considered to obtain reliable estimations of the layer thickness.

ACKNOWLEDGMENTS

This work was supported by the Italian National Program of Antarctic Research (PNRA-WISSLAKE Project). We would like to thank Alessandro Vuan for his constructive suggestions.

REFERENCES

Albarello D. and Lunedei E. (2011). Structure of ambient vibration wavefield in the frequency range of engineering interest ([0.5,20] Hz): Insights from numerical modelling. *Near Surface Geophysics*, **9**, 543–559.

Blankenship D. D., Bentley C. R., Rooney S. T. and Alley R. B. (1986) Seismic measurements reveal a saturated porous layer beneath an active Antarctic ice stream. *Nature*, **322**, 54–57

Blundy J. D. and Sparks R. S. J. (1992) Petrogenesis of mafic inclusions in granitoids of the Adamello Massif, Italy. *J. Petrology*, **33**(5), 1039–1104

Bonnefoy-Claudet S., Cornou C.,Bard P. Y., Cotton F., Moczo P., Kristek J. and Fäh D. (2006) H/V ratio: a tool for site effects evaluation. Results from 1-D noise simulations. *Geophys. J. Int.*, **167**(2), 827–837

Carcione J. M. (2014) *Wave fields in real media: Wave propagation in anisotropic, anelastic, porous and electromagnetic media*. Elsevier, Amsterdam (3rd edition, revised and extended).

D'Amico V., Picozzi M., Baliva F. and Albarello D. (2008) Ambient noise measurements for preliminary site-effects. Characterization in the urban area of Florence. *Bull. Seism. Soc. Am.*, **98**, 1373–1388.

Engelhardt, H., and W. B. Kamb (1997) Basal hydraulic system of a West Antarctic ice stream: Constraints from borehole observations. *J. Glaciol.*, **43**(144), 207–230

García-Jerez, A., Luzón F., Sánchez-Sesma F. J., Lunedei E., Albarello D., Santoyo, M. A. and Almendros, J. (2013) Diffuse elastic wavefield within a simple crustal model. Some consequences for low and high frequencies. *J. Geophys. Res.: Solid Earth*, **118**, 1-19.

Horgan H. J., Anandakrishnan S., Jacobel R. W., Christianson K., Alley R. B., Heeszel D. S., Picotti S. and Jacob I. W. (2012) Subglacial Lake Whillans - Seismic observations of a shallow active reservoir beneath a West Antarctic ice stream. *Earth Planet. Sci. Lett.*, **331–332**, 201–209

Hughes C. J. (1982) *Igneous Petrology*. Elsevier, New York, 551 pp.

Kawase, H., Sánchez-Sesma F. J. and Matsushima S. (2011). The Optimal use of horizontal-to-vertical spectral ratios of earthquake motions for velocity inversions based on diffuse-field theory for plane waves. *Bulletin of the Seismological Society of America*, **101**, 2001–2014.

Kawase, H., Matsushima, S., Satoh T. and Sánchez-Sesma F. J. (2015). Applicability of theoretical horizontal-to-vertical ratio of microtremors based on the diffuse field concept to previously observed data. *Bulletin of the Seismological Society of America*, **105**, 3092–3103.

Konno K. and Ohmachi T. (1998) Ground-motion characteristics estimated from spectral ratio between horizontal and vertical components of microtremor. *Bull. Seism. Soc. Am.*, **88**(1), 228–241

Kramer S. L. (1996) *Geotechnical Earthquake Engineering*. Prentice Hall, New Jersey.

Lay T. and Wallace T. C. (1995) *Modern global seismology*. Academic Press, San Diego, 517 pp.

Lermo J. and F. Chávez García (1993) Site effect evaluation using spectral ratios with only one station. *Bull. Seism. Soc. Am.*, **83**(5), 1574–1594.

Lunedei E. and Albarello D. (2015) Horizontal-to-vertical spectral ratios from a full-wavefield model of ambient vibrations generated by a distribution of spatially correlated surface sources. *Geophys. J. Int.*, **201**, 1140–1153.

Lunedei E. and Malischewsky P. (2015). A review and some new issues on the theory of the H/V technique for ambient vibrations, Chapter 15, in A. Ansal (ed.), *Perspectives on European Earthquake Engineering and Seismology, Geotechnical, Geological and Earthquake Engineering*, **39**, doi: 10.1007/978-3-319-16964-4_15.

Nogoshi M. and Igarashi T. (1971) On the amplitude characteristics of microtremor (part 2). *J. Seism. Soc. Japan*, **24**, 26–40

Peters L. E., Anandakrishnan S., Alley R. B. and Voigt D. E. (2012) Seismic attenuation in glacial ice: A proxy for englacial temperature. *J. Geophys. Res.*, **117**, F02008

Picotti S., Francese R., Giorgi M., Pettenati F. and Carcione J. M. (2016) Estimation of glaciers thickness using the HVSR technique. *J. of Glaciology*, in print

Picotti S., Vuan A., Carcione J. M., Horgan H. J. and Anandakrishnan S. (2015) Anisotropy and crystalline fabric of Whillans Ice Stream (West Antarctica) inferred from multicomponent seismic data. *J. Geophys. Res. Solid Earth*, **120**(6), 4237–4262

Sánchez-Sesma F. J., Rodríguez M., Iturrarán-Viveros U., Luzón F., Campillo M., Margerin L., García-Jerez A., Suarez M., Santoyo M. A. and Rodríguez-Castellanos A. (2011). A theory for microtremor H/V spectral ratio: application for a layered medium. *Geophys. J. Int.*, **186**, 221–225.

Takahashi, R. and Hirano K. (1941). Seismic vibrations of soft ground (in Japanese). *Bulletin of the Earthquake Research Institute*, **19**, 534–543.

Tulaczyk S., Mikucki J. A., Siegfried M. R., Priscu J. C., Barcheck C. G., Beem L. H., Behar A., Burnett J., Christner B. C., Fisher A. T., Fricker H. A., Mankoff K. D., Powell R. D., Rack F., Sampson D., Scherer R. P., Schwartz S. Y. and the Wissard Science Team (2014) WISSARD at Subglacial Lake Whillans, West Antarctica: Scientific operations and initial observations. *Annals of Glaciology*, **55**(65), 51-58

Udias A. (1999) *Principles of seismology*. Cambridge University Press.

van der Baan M (2009) The origin of SH-wave resonance frequencies in sedimentary layers. *Geophys J. Int.*, **178**(3), 1587-1596

Waters K. H. (1978) *Reflection Seismology*. John Wiley and Sons, Inc.

FIGURE CAPTIONS

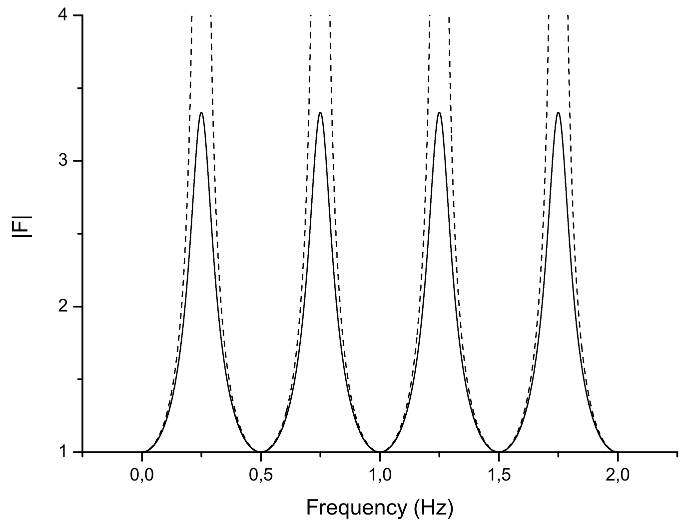

Figure 1. S-wave site amplification in the lossless-elastic (solid line, $Q_1 = \infty$, α = 0.3, Q_2 = 50) and lossless-rigid (dashed line, $Q_1 = \infty$, α = 0) cases.

APPENDIX A: ANALYSIS OF THE TRANSFER FUNCTION AT THE FUNDAMENTAL FREQUENCY

Let us consider the transfer function (2) in the lossless case and analyze its behaviour at the fundamental frequency. Its absolute value is

$$|F| = \left(\cos^2\beta + \alpha^2 \sin^2\beta\right)^{-1/2}, \quad \beta = \frac{\omega h}{v_1}, \tag{A.1}$$

where α is given in equation (4). We have

$$\frac{d|F|}{d\omega} = -\frac{h}{2v_1}\left(\cos^2\beta + \alpha^2 \sin^2\beta\right)^{-3/2}(\alpha^2 - 1)\sin 2\beta. \tag{A.2}$$

The location of the fundamental mode is obtained for $d|F|/d\omega$ = 0, and it is

$$f_0 = \frac{v_1}{4h}. \tag{A.3}$$

The 2nd-order derivative at f_0 is

$$\frac{d^2|F|}{d\omega^2} = \left(\frac{h}{v_1}\right)^2 \frac{\alpha^2 - 1}{\alpha^3}. \tag{A.4}$$

Then if $\alpha \leq 1$ we have a maximum (soft over stiff medium) and $\alpha \geq 1$ gives a minimum (stiff over soft medium). On the other hand, it can easily be shown that $|F|$ = 1 at $f_1 = 2f_0$.

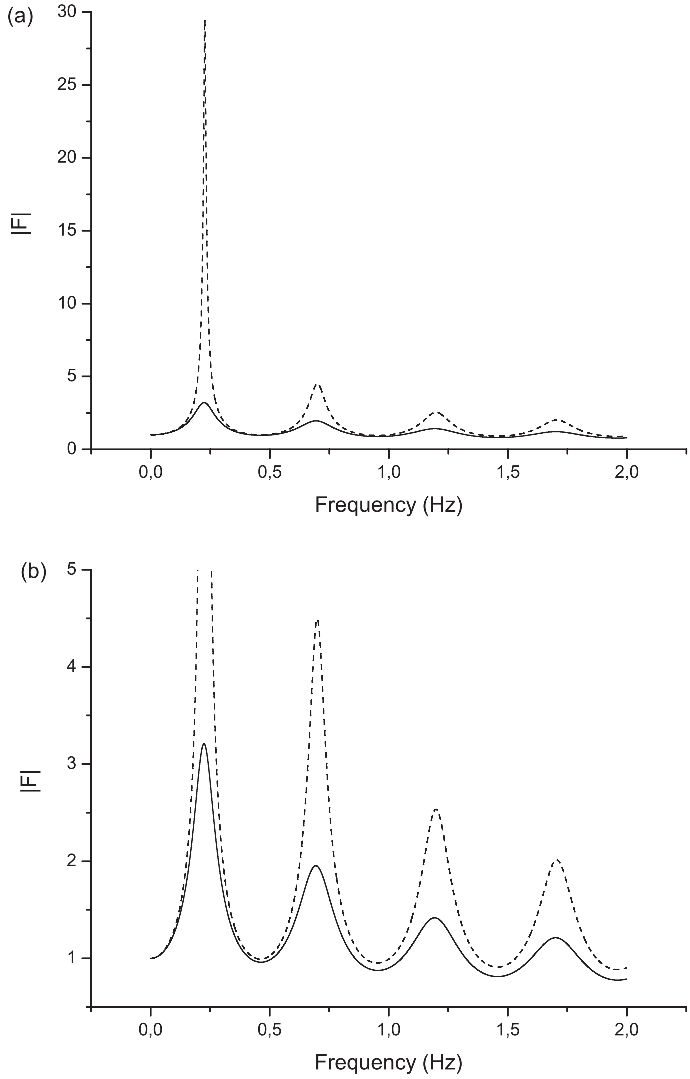

Figure 2. S-wave site amplification in the lossy-elastic case (solid line, Q_1 = 10, α = 0.3, Q_2 = 50) and lossy-rigid case (dashed line, Q_1 = 10, α = 0). Panel (b) shows more details.

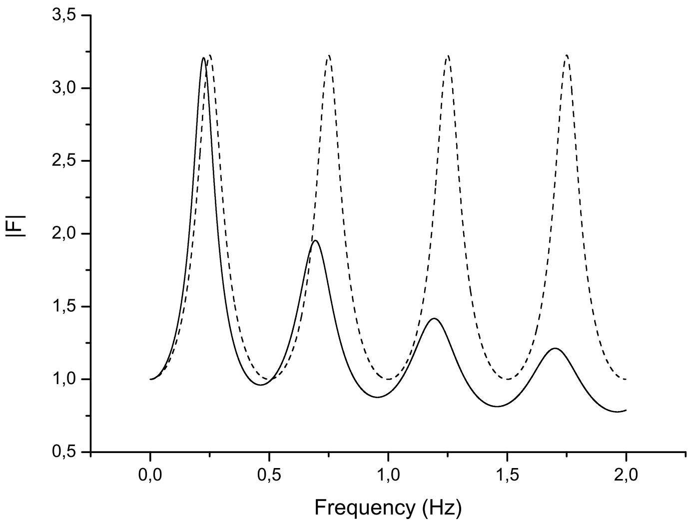

Figure 3. S-wave site amplification in the lossy-elastic case (solid line, Q_1 = 10, α = 0.3, Q_2 = 50) and lossless-elastic case (dashed line, Q_1 = ∞, α = 0.31, Q_2 = ∞).

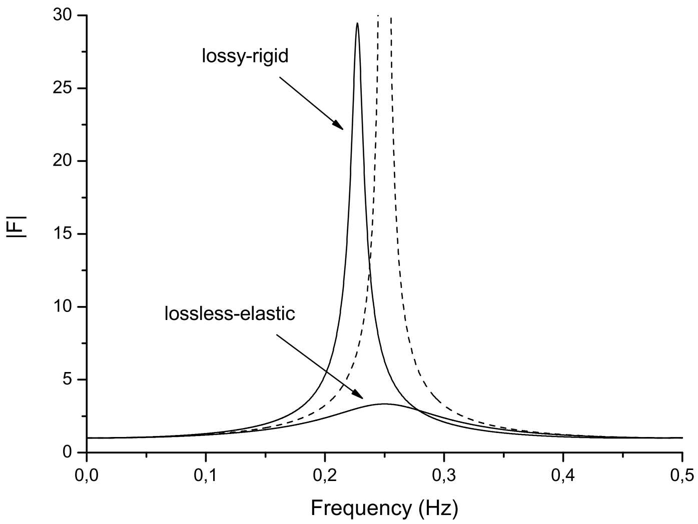

Figure 4. Amplification of the fundamental mode in the lossy-rigid case (Q_1 = 10, α = 0) and lossless-elastic case (Q_1 = ∞, α = 0.3, Q_2 = 50). The dashed line corresponds to the lossless-rigid case.

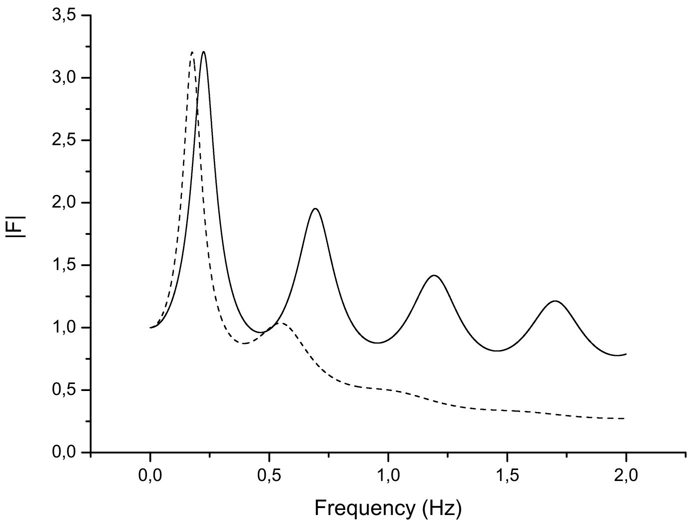

Figure 5. Amplification in the lossy-elastic case (α = 0.3) for Q_1 = 10 (solid line) and Q_1 = 3 (dashed line) (Q_2 = 50).

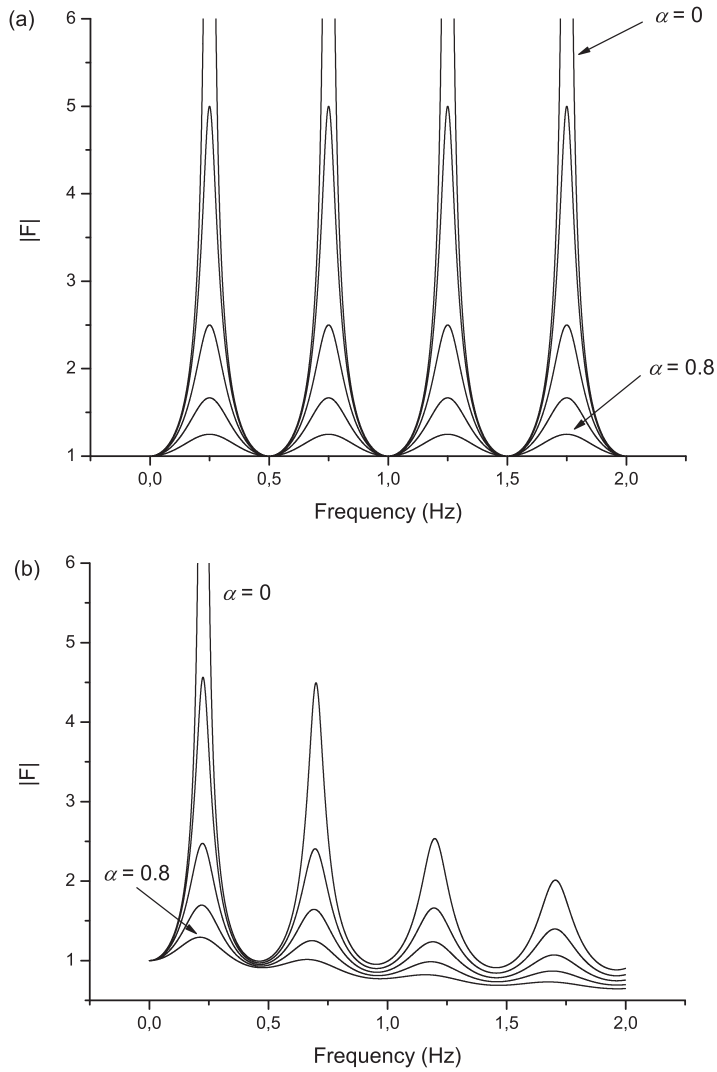

Figure 6. Amplification in the lossless (a) and lossy (b) cases for different values of the impedance contrast α (0, 0.2, 0.4, 0.6 and 0.8), corresponding to the fundamental mode. In (a) it is $Q_1 = Q_2 = \infty$, while in (b) it is $Q_1 = 10$ and $Q_2 = 50$.

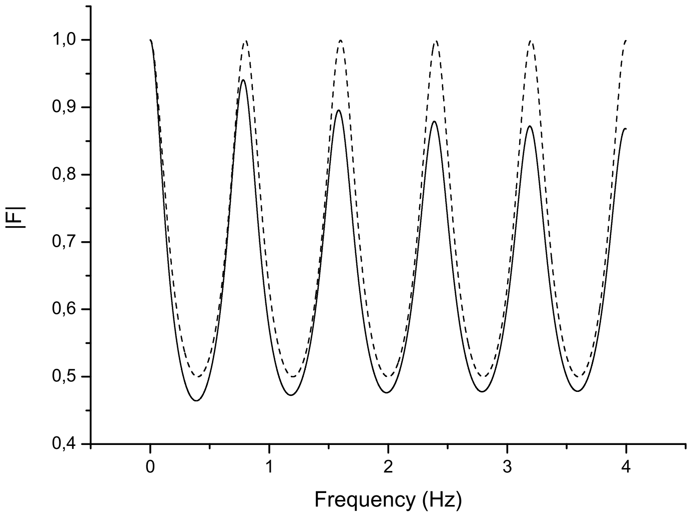

Figure 7. Amplification in the lossless case (dashed line, Q_1 = 50, $Q_2 = \infty$) and lossy case (solid line, Q_1 = 50, Q_2 = 10) for α = 2. The lower half-space is softer than the layer, such that c_{U1} = 1.6 km/s, ρ_1 = 2.5 g/cm^3, c_{U2} = 1 km/s and ρ_2 = 2 g/cm^3.

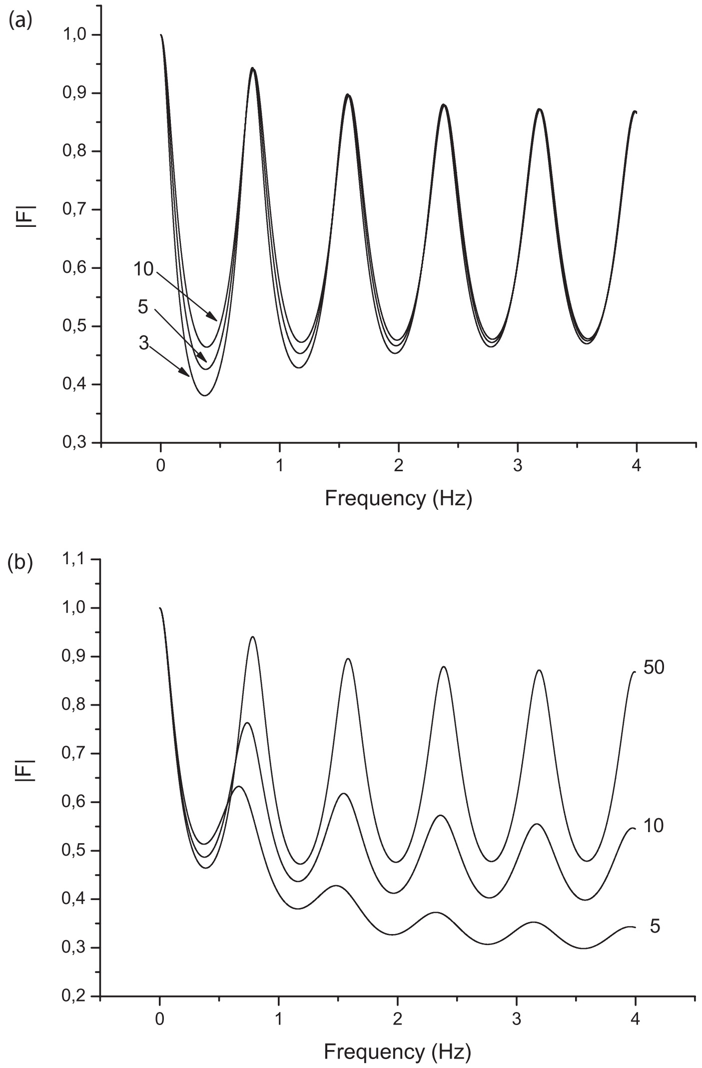

Figure 8. Amplification in the lossy case (Q_1 = 50 in (a) and Q_2 = 10 in (b)) for α = 2. The number indicates the quality factor of the half-space (a) and layer (b), respectively.

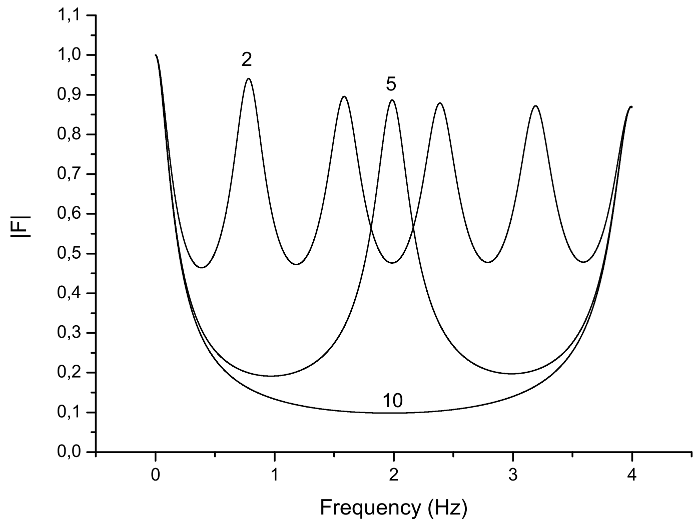

Figure 9. Amplification function in the lossy case for α = 2, 5 and 10 (Q_1 = 50 and Q_1 = 10).

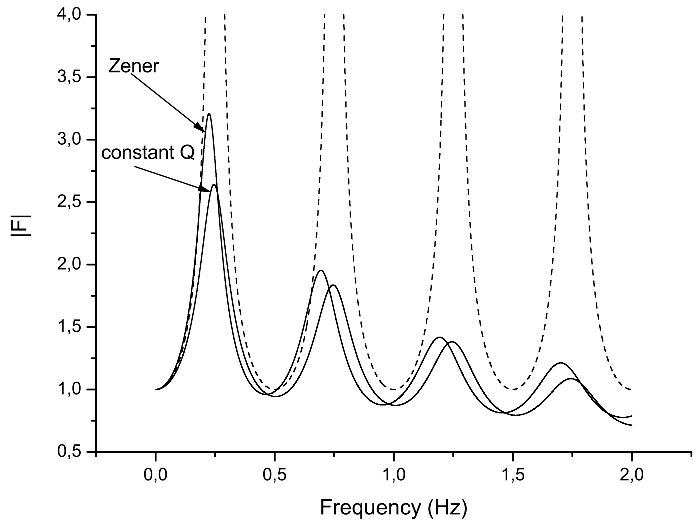

Figure 10. Amplification in the lossy-elastic (solid line, Q_1 = 10, Q_2 = 50, α = 0.3). Attenuation is described by the Zener model and the constant-Q model (the two solid lines). The dashed line corresponds to the lossless-rigid case ($Q_1 = \infty$, α = 0).

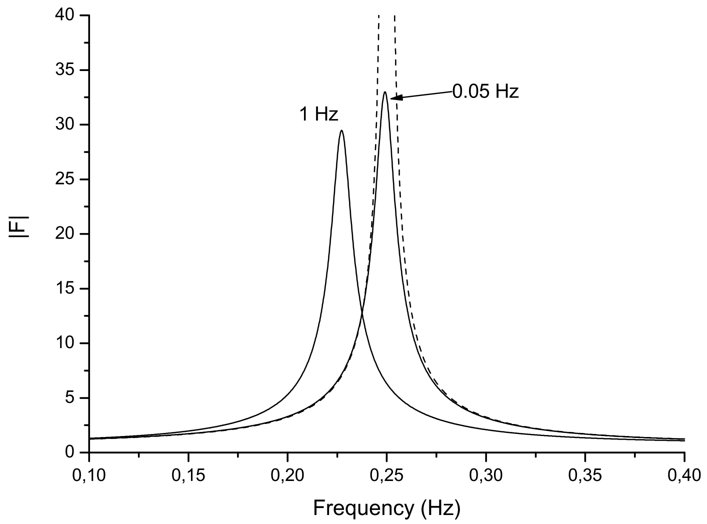

Figure 11. Amplification in the lossy-rigid (solid lines, $Q_1 = 10$, $\alpha = 0$) and lossless-rigid (dashed line, $Q_1 = \infty$, $\alpha = 0$) cases, corresponding to the fundamental mode. The numbers indicate the location of the Zener relaxation peak.

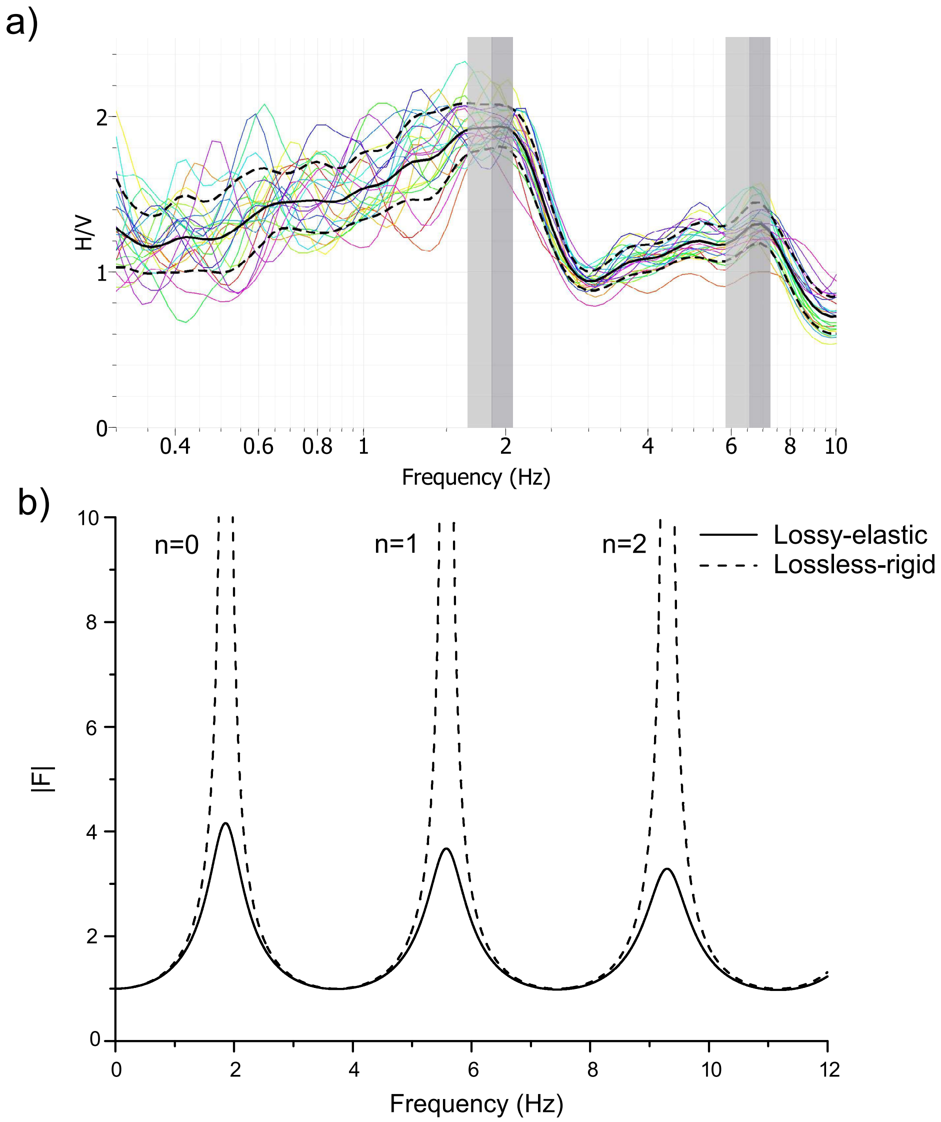

Figure 12. Experimental H/V response (a) and theoretical amplification functions (b) corresponding to the Pian di Neve glacier (Adamello massif, Northen Italy). The grey vertical bars quantify the experimental error associated to the resonance frequency of the fundamental (1.85 ± 0.3 Hz) and first higher mode (6.54 ± 0.7 Hz). The theory predicts the measured fundamental-mode resonance frequency both for the lossy-elastic and lossless-rigid models.

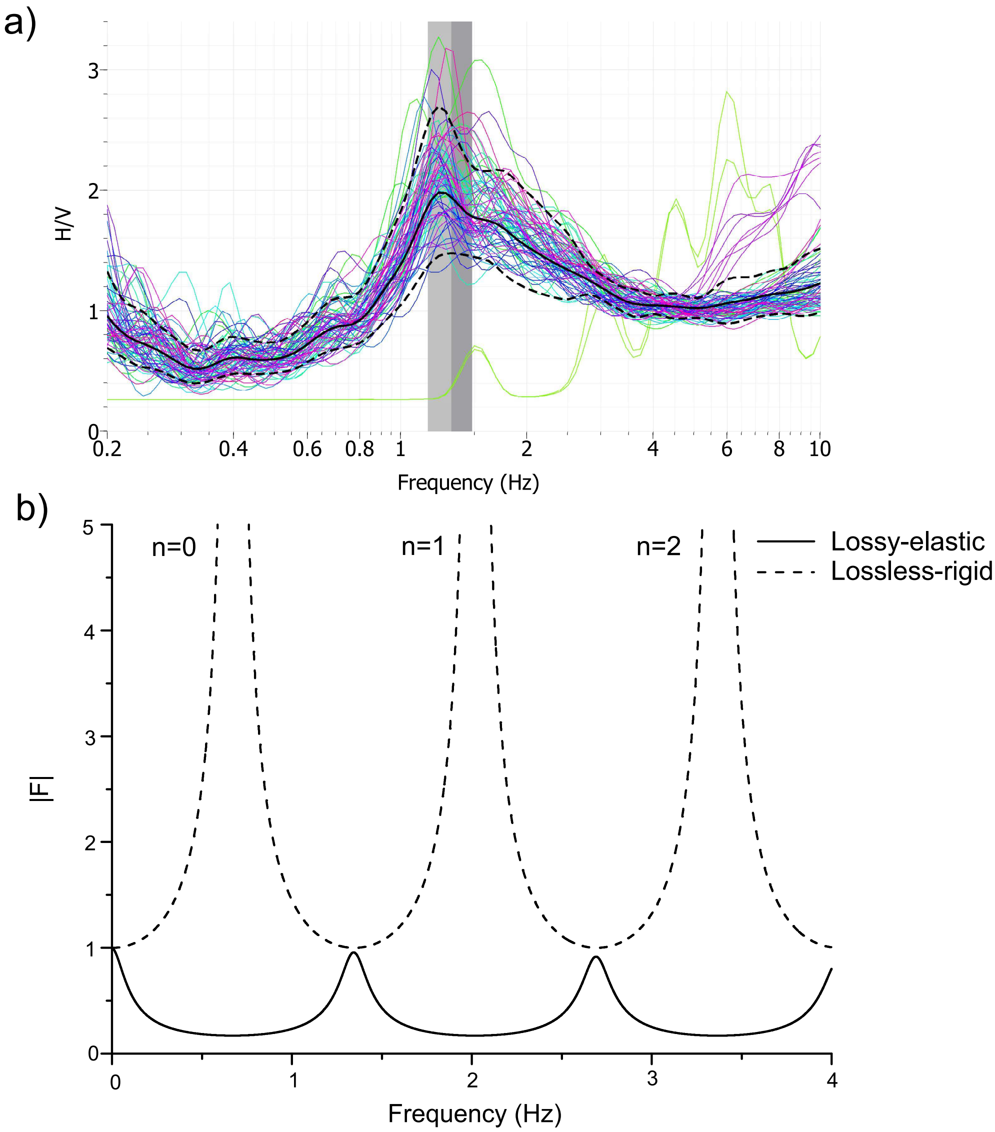

Figure 13. Experimental H/V response (a) and theoretical amplification functions (b) corresponding to the Whillans Ice Stream (West Antarctica). The grey vertical bars quantify the experimental error associated to the resonance frequency of the fundamental mode (1.3 ± 0.2 Hz). The theory predicts the measured fundamental-mode resonance frequency only for the lossy-elastic model.